HHS Public Access

Author manuscript

Mol Pharm. Author manuscript; available in PMC 2022 November 11.

Published in final edited form as:

Mol Pharm. 2022 May 02; 19(5): 1573–1585. doi:10.1021/acs.molpharmaceut.2c00058.

Cowpea Mosaic Virus Outperforms Other Members of the Secoviridae as In Situ Vaccine for Cancer Immunotherapy

Veronique Beiss,
Departments of NanoEngineering, University of California San Diego, La Jolla, California 92093, United States

Chenkai Mao,
Department of Microbiology and Immunology, and Norris Cotton Cancer Center, Geisel School of Medicine at Dartmouth and Dartmouth Hitchcock Health, Lebanon, New Hampshire 03756, United States

Steven N. Fiering,
Department of Microbiology and Immunology, and Norris Cotton Cancer Center, Geisel School of Medicine at Dartmouth and Dartmouth Hitchcock Health, Lebanon, New Hampshire 03756, United States

Nicole F. Steinmetz
Departments of NanoEngineering, Departments of Radiology, Departments of Bioengineering, Moores Cancer Center, Center for Nano-ImmunoEngineering, and Institute for Materials Discovery and Design, University of California San Diego, La Jolla, California 92093, United States; Department of Microbiology and Immunology, and Norris Cotton Cancer Center, Geisel School of Medicine at Dartmouth and Dartmouth Hitchcock Health, Lebanon, New Hampshire 03756, United States

Abstract

In situ vaccination for cancer immunotherapy uses intratumoral administration of small molecules, proteins, nanoparticles, or viruses that activate pathogen recognition receptors (PRRs) to reprogram the tumor microenvironment and prime systemic antitumor immunity. Cowpea mosaic virus (CPMV) is a plant virus that—while noninfectious toward mammals—activates mammalian

Corresponding Author: Nicole F. Steinmetz – Departments of NanoEngineering, Departments of Radiology, Departments of Bioengineering, Moores Cancer Center, Center for Nano-ImmunoEngineering, and Institute for Materials Discovery and Design, University of California San Diego, La Jolla, California 92093, United States; Department of Microbiology and Immunology, and Norris Cotton Cancer Center, Geisel School of Medicine at Dartmouth and Dartmouth Hitchcock Health, Lebanon, New Hampshire 03756, United States; nsteinmetz@ucsd.edu.

The authors declare the following competing financial interest(s): Drs. Steinmetz and Fiering are co-founders of, have equity in, and have a financial interest with Mosaic ImmunoEngineering Inc. Dr. Fiering serves as scientific advisor and paid consultant to Mosaic; Dr. Steinmetz serves as Director, Board Member, and Acting Chief Scientific Officer, and paid consultant to Mosaic. The other authors declare no potential conflicts of interest.

Supporting Information

The Supporting Information is available free of charge at https://pubs.acs.org/doi/10.1021/acs.molpharma-ceut.2c00058.
Genome organization of CPMV; RNA and protein homology analysis comparing CPMV, CPSMV, and TRSV; TRSV infected plant; CPMV-vimentin interactions; efficacy of CPMV-ISV in presence of anti-vimentin antibodies; VOPBA with CPMV and Qβ nanoparticles conjugated with vimentin-binding peptides; supporting methods (PDF)

Complete contact information is available at: https://pubs.acs.org/10.1021/acs.molpharmaceut.2c00058

PRRs. Application of CPMV as in situ vaccine (ISV) results in a potent and durable efficacy in tumor mouse models and canine patients; data indicate that CPMV outperforms small molecule PRR agonists and other nonrelated plant viruses and virus-like particles (VLPs). In this work, we set out to compare the potency of CPMV versus other plant viruses from the Secoviridae. We developed protocols to produce and isolate cowpea severe mosaic virus (CPSMV) and tobacco ring spot virus (TRSV) from plants. CPSMV, like CPMV, is a comovirus with genome and protein homology, while TRSV lacks homology and is from the genus nepovirus. When applied as ISV in a mouse model of dermal melanoma (using B16F10 cells and C57Bl6J mice), CPMV outperformed CPSMV and TRSV—again highlighting the unique potency of CPMV. Mechanistically, the increased potency is related to increased signaling through toll-like receptors (TLRs)—in particular, CPMV signals through TLR2, 4, and 7. Using knockout (KO) mouse models, we demonstrate here that all three plant viruses signal through the adaptor molecule MyD88—with CPSMV and TRSV predominantly activating TLR2 and 4. CPMV induced significantly more interferon β (IFNβ) compared to TRSV and CPSMV; therefore, IFNβ released upon signaling through TLR7 may be a differentiator for the observed potency of CPMV-ISV. Additionally, CPMV induced a different temporal pattern of intratumoral cytokine generation characterized by significantly increased inflammatory cytokines 4 days after the second of 2 weekly treatments, as if CPMV induced a “memory response”. This higher, longer-lasting induction of cytokines may be another key differentiator that explains the unique potency of CPMV-ISV.

Graphical Abstract

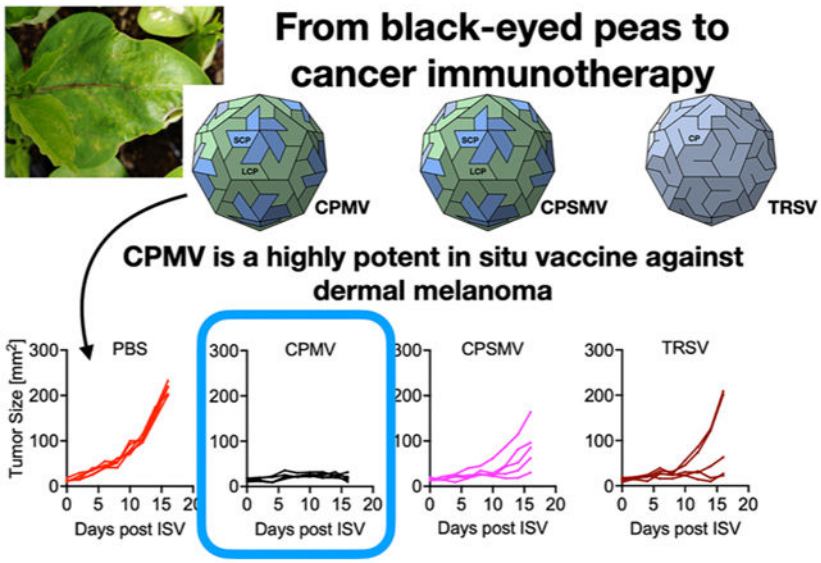

Keywords

plant virus; secoviridae; cowpea mosaic virus; in situ vaccine; cancer immunotherapy

INTRODUCTION

Cancer immunotherapy is a form of cancer therapy that targets the patient's own immune system to recognize and eliminate tumors and metastatic disease. Unlike conventional treatments such as surgery, chemotherapy, or radiation, cancer immuno-therapy holds the potential to induce not only potent antitumor immunity but also to elicit long lasting, durable responses, and immune memory to protect patients from outgrowth of metastatic disease or recurrence.[1,2] There are several classes of cancer immunotherapies and treatment regimens including cell-based therapies such as CAR-T cells[3] or virus-based therapies such as oncolytic viruses and/or gene delivery vectors that are programmed to induce cancer cell death and/or to express immunomodulatory cytokines to modulate the tumor microenvironment (TME).[4,5] Viral vectors have also been engineered to express tumor-associated antigens (TAAs) or neoantigens to function as cancer vaccines.[6,7] Newer classes of virus-based therapeutics are plant virus nanoparticles and virus-like particles (as detailed below). Another category of cancer immunotherapies are antibodies, for example, those targeting immune checkpoints[8] as well as small molecule therapeutics, for example, those that bind and activate pathogen recognition receptors (PRRs).[9,10]

One branch of cancer immunotherapy is referred to as in situ vaccination—here the immunostimulatory agent is administered directly into an identified solid tumor to reverse immunosuppression and recruit and activate innate immune cells to induce cancer cell killing and processing of TAAs or neoantigens—processes that ultimately prime systemic anti-tumor immunity.[11] The development pipeline for novel reagents and drug candidates that function as ISV is rapidly developing: examples of oncolytic viruses that are already approved for therapy or are undergoing clinical trials are Imlygic (a herpes-based therapeutic), Reolysin, a reovirus-based therapeutic, and PVSRIPO, an engineered polio virus.[12,13] Small molecule PRR agonists such as Imiquimod[14] and nanoparticle formulations delivering CpG (a Toll-like receptor (TLR) 9 agonist) are also approved or progressing through clinical trials.[15]

Our research has focused on the development of plant viruses as nanoparticles for use as ISV. One plant virus nanoparticle stands out in terms of its efficacy: cowpea mosaic virus (CPMV) demonstrates potent and long-lasting efficacy against tumors and metastatic disease and is being developed as a drug candidate for translation into the clinic. While noninfectious toward mammals, plant viruses such as CPMV present pathogen-associated molecular patterns and therefore activate PRRs. We demonstrated that nanoparticles from CPMV upon intratumoral injection (i.e., used as ISV) stimulate a potent antitumor immune response in mouse models of melanoma, ovarian cancer, breast cancer, colon cancer, and glioma.[16–18] CPMV-ISV induces durable immune-mediated antitumor efficacy and immunological memory to prevent cancer recurrence. Most importantly, translation of CPMV-ISV to clinical trials in companion dogs with melanoma, breast cancer, and sarcoma demonstrate potent antitumor efficacy of this approach.[19–21] Mechanistically, CPMV-ISV modulates the TME by signaling through PRRs, such as TLRs. CPMV forms a nonglycosylated 30 nm-sized icosahedral capsid with a bipartite RNA genome. We have shown that both, the capsid and RNA, contribute to the immunostimulatory effect of CPMV: the encapsidated RNA signals through TLR7 and the capsid protein signals through TLR2

and 4; RNA-containing CPMV is more potent compared to RNA-free VLPs and this can be explained by additional signaling through TLR7 leading to type I interferon secretion.[22,23] CPMV-ISV activates innate immune cells (switch of M2 to M1 macrophages, recruits and activates of Natural Killer cells, dendritic cells, and N1 neutrophils), thereby initiating a cascade of tumor cell killing mechanisms, resulting in efficient presentation of both TAAs and neoantigens and generation of a functionally active adaptive antitumor immunity via tumor antigen-specific $CD4^+$ and $CD8^+$ effector and memory T cells.[22,24] We have demonstrated efficacy of CPMV as solo-treatment and in combination with radiation,[25] chemotherapy,[26] and checkpoint inhibitors.[27]

Importantly, we found that CPMV has unique potency when used as ISV, that is, used as immunostimulatory agent administered directly into a tumor, compared to other nonrelated plant viruses, bacteriophage VLPs or mammalian VLPs,[28] or small molecule adjuvants[17,29] in terms of immune activation mechanisms and antitumor efficacy. Specifically, we compared efficacy and mechanism of immune activation of CPMV versus tobacco mosaic virus,[16] potato virus X,[30] cowpea chlorotic mottle virus, physalis mosaic virus-like particles, sesbania mosaic virus, Qβ phage VLPs, and Hepatitis B core particles[28]—and data show while all virus-based nanoparticles are immunogenic, only CPMV-ISV primes potent antitumor immunity. In the prior work, CPMV was compared with other viruses of distinct size and shape as well as similar size and structure yet lacking homology—therefore in this work, we set out to compare the efficacy of intratumorally injected CPMV with related plant viruses, namely, cowpea severe mosaic virus (CPSMV) and tobacco ringspot virus (TRSV). CPSMV and CPMV belong to the genus comovirus and TRSV is a nepovirus—both of which belong to the family of the Secoviridae and the order of the Picornavirales.

We developed scalable molecular farming approaches to produce CPSMV and TRSV alongside with CPMV in cowpea plants. We characterized the plant virus nanoparticles and probed their interaction with vimentin—because CPMV has been shown to uniquely bind to the mammalian protein vimentin,[31] a cytoskeletal protein involved in a myriad of cellular functions, which can be surface-expressed or secreted in tumor cells, endothelial cells, and immune cells—in particular at sites of inflammation or disease. We tested and compared the efficacy of intratumoral injected CPSMV and TRSV vs CPMV in a murine dermal melanoma model and investigated the mechanism of immune activation.

METHODS

Model of CPSMV.

The protein structure of CPSMV has not yet been reported. However, given the structural and sequence homology between CPMV and CPSMV, we built a homology model between the coat proteins of CPMV and CPSMV using MODELLER (salilab.org/modeller) software —from there, using the spatial parameters of CPMV, the CPSMV virus capsid was build using Chimera.[32,33]

Viral Nanoparticle Propagation and Purification.

CPMV was propagated in and purified from *V. unguiculata* as described in ref 34. For propagation and purification of CPSMV and TRSV, the exact same methods were applied with the addition of TRSV being propagated in *V. unguiculata* as well as in *N. tabacum*. In brief, *V. unguiculata* plants were infected with plant viruses at 8 days. Leaf harvest occurred at 10–12 days after infection for CPMV, 8–10 days after infection for CPSMV, and 4–6 days after infection for TRSV, when disease was clearly established and just before wilting of the leaves occurred. For propagation of TRSV in *N. tabacum*, *N. tabacum* was germinated and grown in soil and infected at around 4 weeks. Infected leaves were harvested within 20 days and stored at −80 °C until further processing. For purification, leaves were homogenized in a blender with 0.1 M potassium phosphate buffer pH 7.0 and clarified through filtration; plant viruses were purified through chloroform/butanol extraction and PEG precipitation followed by ultracentrifugation over a sucrose gradient; the light scattering bands were isolated and virus particles were collected by ultracentrifugation over a sucrose gradient. Pure virus nanoparticles were then stored in 0.1 M potassium phosphate buffer pH 7.0 at 4 °C until further use.

Characterization of CPMV, CPSMV, and TRSV.

Purified virus nanoparticles were quantified using UV/vis spectroscopy and BCA assay and characterized by agarose gel electrophoresis using 1.2% (w/v) agarose gels in 1× TBE buffer, denaturing sodium dodecyl sulfate-polyacrylamide gel electrophoresis (SDS-PAGE) using 4–12% Nu-PAGE gels (Invitrogen), transmission electron microscopy (TEM) using a Tecnai TEM at 80 kV and uracyl acetate-stained (2% (w/v)) samples, size exclusion chromatography (SEC) using a Superose 6 column and ÄKTA explorer (GE Healthcare), as well as dynamic light scattering using a Zetasizer Nano ZSP/Zen5600 instrument (Malvern Panalytical). Detailed methods are as described in ref 35.

Immunization of Mice Using CPMV, CPSMV, and TRSV.

All mouse studies performed were approved by the Institutional Animal Care and Use Committees of the University of California San Diego and Dartmouth College. To generate antibodies against the three plant viruses CPMV, CPSMV, and TRSV, mice were immunized in a prime-boost regiment with one prime and two boosts, each 14 days apart. Female C57Bl6J mice (6–8 weeks old) were obtained from Jackson laboratory. Mice were immunized subcutaneously by injecting 100 μg/30 μL of each virus or 30 μL PBS on day 0, 14, and 28. Mice were bled after each immunization by tail vein bleed and final heart blood was taken 1 week after the last boost (day 35). Tail vein bleeds were diluted 1:10 in PBS and the blood frozen at −20 °C until further use. The final bleed was collected in lithium-heparin-treated tubes. Plasma from all bleeds was collected by centrifugation at 1500*g* for 10 mins at room temperature and kept at −20 °C until further use.

To investigate the antibody response against the three plant viruses, a direct ELISA was performed. In 96 well plates, 100 μg/well CPMV, CPSMV, or TRSV were coated for 1 h, at room temperature. Plates were washed three times with PBS-T [PBS + 0.5% (v/v) Tween-20] using 200 μL/well between each step. Plates were blocked for 1 h, at room temperature using 5% (w/v) milk powder in PBS. After washing, twofold serial dilutions

of plasma samples from immunized animals, ending at a dilution of 1:512 000, in PBS were added and incubated for 1 h, at room temperature. After washing, an HRP-labeled goat-anti-mouse IgG secondary antibody (Thermo Fisher Scientific) diluted 1:5000 in PBS was added (100 μL/well) and incubated for 1 h, at room temperature. After a final washing step, 100 μL/well of 1-Step Ultra TMB substrate was added and developed for 30 mins in the dark and absorbance read at 450 nm on a Tecan microplate reader. The endpoint antibody titers were defined as the absorbance exceeding two times the background value (blank wells without the plasma sample).

Cross-Reactivity between Murine Sera against Plant Viruses.

Murine sera against each plant virus were obtained through immunization of mice (see above) and tested for potential cross-reactivity against the other plant viruses. For this, 6 μg of CPMV, CPSMV, or TRSV was separated on SDS-PAGE and transferred onto the nitrocellulose membrane followed by western blot. All wash steps in between incubations were done with PBST (PBS with 0.05% (v/v) Tween-20), membranes were washed three times at room temperature, and all incubation steps were done for 1 h at room temperature. First, the membrane was blocked in 5% (w/v) milk powder in PBS, washed, and incubated in αCPMV, αCPSMV, or αTRSV mouse sera, respectively, 1:1000 in PBS. After washing, the membrane was incubated with a HRP-labeled goat anti-mouse IgG (Thermo Fisher Scientific), 1:5000 in PBS. After a final wash, the DAB substrate [3,3′-diaminobenzidine; DAB Susbtrate Kit, Peroxide (HRP), Vector Laboratories] was added to the membrane and incubated for 1–5 mins or until bands were visible. The reaction was stopped with water and the membranes immediately imaged under white light with a FluorChem R imaging system (Protein Simple).

Vimentin Binding via Virus Overlay Binding Protein Assay.

To assess binding of plant viral nanoparticles to vimentin, a Virus Overlay Binding Protein Assay (VOBPA) was performed as previously described in ref 31. Two versions of the VOBPA were performed: a VOBPA via western blot and a VOBPA dot blot. Briefly, for the VOBPA via western blot, 10 μg of vimentin was loaded onto 4–12% Nu-PAGE gels in 1xMOPS, subsequently transferred to a nitrocellulose membrane, denatured and renatured, and then blocked using 5% (v/v) milk powder in PBS followed by incubation with 2 μg mAbV9 (eBioscience or ThermoFisher) or mAb84–1 (CSV84–1, Abnova) or 100 μg CPMV, CPSMV or TRSV, respectively. For VOBPA dot blots, 10 μg of vimentin was dotted onto a nitrocellulose membrane and the blocked membrane was incubated with 2 μg mAbV9 or mAb84–1 or 100 μg CPMV, CPSMV, or TRSV, respectively. For the dot blot, vimentin did not undergo the denaturing and renaturing process. CPMV, CPSMV, or TRSV were detected using sera from mice followed by staining with a HRP-labeled goat anti-mouse IgG 1:5000 in PBS (Thermo Fisher Scientific); detection was carried out using the DAB/Ni Peroxidase Substrate Kit (Vector Biolabs). Membranes were stained under white light using a FluorChem R imaging system (Protein Simple).

Tumor Model and In Situ Vaccination.

All mouse studies performed were approved by the Institutional Animal Care and Use Committees of the University of California San Diego and Dartmouth College. B16F10

cells (ATCC CRL-6475, mouse skin melanoma) were cultured to 80% confluency in Dulbecco's modified Eagle medium with L-glutamine, supplemented with 1% (v/v) penicillin/streptomycin and 10% (v/v) fetal bovine serum (FBS) at 37 °C and 5% CO_2. Cells were harvested by trypsin digestion and collected by centrifugation at 150*g* for 5 min. Cells were resuspended in PBS and 1.25×10^5 B16F10 cells in 30 μL of PBS were implanted orthotopically into female C57Bl6 mice (6–8 weeks old, The Jackson Laboratory) skin by intradermal injection. For in situ vaccination, tumors were treated by intratumoral administration of 100 μg of CPMV, CPSMV, or TRSV in 30 μL of PBS; PBS was used as a control group. Tumor growth was monitored every other day by caliper. Weight was measured every other day. Mice were euthanized when the tumor size reached 200 mm^2 or were observed till 30 days after treatment.

Data are presented as the average means ± standard error of the means (SEM). The results shown here are representative responses from multiple experiments, which are repeated at least once with similar results. *T*-test *p*-values < 0.05 were required to assign significance and are represented as an asterisk (*) in the figures and $p < 0.01$ as **, and $p < 0.001$ as ***. Flank tumor growth curves were analyzed using two-way ANOVA, with $p > 0.05$ as not significant (ns), $p < 0.05$ as *, $p < 0.01$ as **, and $p < 0.001$ as ***.

Immunological Assays.

Tumor draining lymph node (DLNs) from B16F10-bearing mice treated with CPMV, CPSMV, or TRSV were harvested and lymphocytes were extracted. The extracted lymphocytes were then cultured at 2×10^6 cells/mL per well using 96-well plates and in RPMI 1640 medium (Invitrogen, Carlsbad, CA, USA) supplemented with 10% (v/v) FBS and 1% (v/v) penicillin/streptomycin at 37 °C and 5% CO_2. PBS or 12 μg/mL CPMV, CPSMV, or TRSV in 250 μL medium were added. The cell culture supernatant (referred to as conditioned medium) was collected 24 h later by centrifugation of the cell mixture, and the conditioned medium was collected and stored frozen (–20 °C) for cytokine quantification. Conditioned medium was analyzed by enzyme-linked immunosorbent assay (ELISA) to detect interleukin-6 (IL-6), interferon γ (IFN-γ), and interferon β (IFN-β) (BioLegend).

Female C57BL/6J or C57BL/6J background knockout mice (KO) for MyD88−/−, TLR2−/−, TLR4−/−, TLR5−/−, TLR7−/−, and TLR9−/− mice (6–8 weeks old) were purchased from The Jackson Laboratory and bred at Dartmouth College. Splenocyte assays established previously[22] were set up using these different mouse strains. Briefly, splenocytes were cultured with either CPMV, CPSMV, or TRSV and cytokines were quantified by ELISA to detect IL-6, interferon γ (IFN-γ), and interferon β (IFN-β).

Data are presented as the mean ± standard error of the mean (SEM). The results shown here are representative responses from biological triplicates. *T*-test *p*-values < 0.05 were required to assign significance and are represented as an asterisk (*) in the figures and $p < 0.01$ as **, and $p < 0.001$ as ***.

RESULTS AND DISCUSSION

Homology between CPMV, CPSMV, and TRSV.

CPMV has a bipartite positive-sense ssRNA genome, consisting of RNA-1 and RNA-2.[36,37] The RNA segments are encapsidated separately in isometric particles, described as bottom (B; which contains RNA-1) and middle (M; which contains RNA-2) components. Both components, or the RNA isolated from them, are required to be present in a cell for productive infection.[38] Each RNA molecule is covalently linked to a small basic protein (VPg: viral protein genome-linked) at its 5′ terminus[39,40] and polyadenylated at the 3′ end[41] (Figure S1A). Both RNA molecules contain one large open reading frame (ORF) and are translated into precursor polyproteins, which are subsequently cleaved in cis and trans by a virus-encoded proteinase.[42–44] In general, the larger RNA-1 (5889 nt) encodes the virus replication machinery[45] as well as the virus-specific proteinase and the VPg, which has an essential role in the initiation of RNA synthesis.[43] The smaller RNA-2 (3481 nt) encodes two capsid proteins and the movement protein (MP) that enables passage through the plasmodesmata between cells. The most obvious function of the capsid proteins is the protection of the RNA, but they also have a role in short-range cell-to-cell spread and in long-distance movement of the virus via the vascular bundle system.[44,46,47] By isopycnic centrifugation on density gradients, CPMV particles can be separated into three components (Figures 1 and S1B), which have identical protein composition but differ in their RNA contents.[38,48,49] The particles of the top (T) component are devoid of RNA, while the M and B components each contain a single RNA molecule, RNA-2 and RNA-1, respectively.[50] It should be noted that the T component, which makes a small fraction of CPMV, is not collected in our purification process—only the light scattering bands from M and B components are collected. Therefore, the CPMV ISV reagents include equal amounts of B and M components.

The overall genome organization of CPSMV and TRSV follows the genome organization of CPMV—all three plant viruses have a bipartite, positive-sense ssRNA genome. RNA-1 encodes proteins involved in replication, and RNA-2 encodes structural proteins and proteins necessary for cell-to-cell and long-distance movement. Each RNA segment has a VPg (genome-linked viral protein) attached to the 5′ end and a poly-A tail at the 3′ end (Figure 1). The CPSMV RNA-1 measures 5957 nts (NC_003545.1) and RNA-2 measures 3732 nts (NC_003544.1).[51,52] RNA sequence alignment indicates homology between CPMV and CPSMV—BLAST search indicates similarities covering 10% of the sequence, principally with 70% identities identified in the MP and large coat protein (L-CP) ORFs (Figure S2A). Similarities were also apparent for RNA-1 with identities covering 26% of the genome—identities ranging from 65 to 71% were identified within the coding region for the RNA-dependent RNA polymerase (RdRp) and the 58 K protein (Figure S2B). The TRSV RNA-1 measures 7514 nts (NC_005097.1) and RNA-2 measures 3929 nts (NC_005096.1).[53] A blast search indicates no significant homology between the genome sequences of TRSV and CPMV.

Finally, we performed homology analysis among the CPMV, CPSMV, and TRSV coat proteins. All three viral capsids have pseudoT or pT = 3 symmetry and form three isometric

particles denotated as T, M, and B components. It should be noted that the B component of TRSV contains a mixture of particles containing the longer RNA-1 or two copies of RNA-2. There is no homology between the CPMV and TRSV coat proteins (AAO15596.1, 515 aa)—this is as expected given that CPMV has a S and L protein and TRSV a single coat protein. There is significant homology between S and L proteins of CPMV and CPSMV (Figure S3). Specifically, the S proteins of CPMV (189 aa, 1NY7_1) and CPSMV (195 aa, NP_734065.1) have 35% identities (amino acid match) and 65% positives (similarities in amino acid compositions and positions); the L proteins of CPMV (369 aa, 1NY7_2) and CPSMV (195 aa, NP_734064.1) have 49% identities and 66% positives in sequence homology. While all three plant viruses belong to the family of the Secoviridae and the order of the Picornavirales, by homology, CPMV and CPSMV are closely related, while TRSV is not a close relative of either.

CPMV, CPSMV, and TRSV Propagation in Planta, Purification, and Characterization.

CPMV and CPSMV were propagated in and purified from *V. unguiculata* (cowpea) and TRSV was propagated in *V. unguiculata* as well as in *N. tabacum* (tobacco). While propagation of TRSV was successful in both *V. unguiculata* and *N. tabacum*, we carried forward with propagation of TRSV in cowpeas for two reasons: (1) the growth cycle of cowpeas is significantly faster than tobacco—that is from seed to infection and harvest of leaves takes 3–4 weeks for cowpea vs ~ 3 months for tobacco and (2) production of all three plant viruses in the same host allows us to rule out differences in efficacy or immune activation due to differences in potential host components in the preparations.

For cowpeas infected with CPMV and CPSMV, symptoms were more severe for CPSMV vs CPMV infection—as the name suggests. For CPMV-infected plants, yellow chlorotic or mottling spots were observed on the primary leaves. Trifoliates infected with CPMV developed bright yellow or light green spots with little leaf distortion observed. Vein discoloration was not observed for CPMV-infected plants. For CPSMV-infected primary leaves, lesions appear smaller than those observed for CPMV, and the lesions appear as yellow to red-brown necrotic spots (signs of necrosis). Veins also appear discolored with red-brown appearance and the trifoliates—if they develop and grow—appeared severely blistered and distorted (Figure 2).

TRSV was propagated in *V. unguiculata* as well as in *N. tabacum* and showed the typical ring spot symptoms on the primary leaves (Figures 2 and S4). In cowpeas, TRSV infection resulted in necrotic lesions in primary leaves and systemic necrosis and leaf wilting. The lesions were red-brown colored with veins turning the same color. TRSV infection leads to stem wilting and mostly prevents trifoliates from development in cowpeas. In tobacco plants, TRSV causes lesions as rings or spots on primary infected leaves; the trifoliates showed rings or lines. Symptoms in tobacco plants were less severe compared to cowpeas.

Highest yields were obtained for CPMV with 0.5–0.9 mg purified CPMV per gram of freshly harvested infected leaf material; CPSMV was purified at yields of 0.2–0.5 mg CPSMV per gram infected leaf material, and TRSV has lower yields ranging between 0.05 and 0.2 mg/g leaf tissue (independent of the production host, cowpea vs tabacco). However, it should be noted that propagation and purification could be further optimized to achieve

increased yields. For example, in preliminary studies, we examined TRSV propagation at 25 °C vs 22 °C, and plants infected with TRSV and maintained at lower temperatures experienced less or delayed leaf wilting and a lower degree of necrosis (which is associated with the plant immune response against plant viruses[54]), therefore allowing higher virus titers to accumulate in the plants.

The purified viral nanoparticles were then characterized to confirm their structural integrity and purity: CPMV and CPSMV capsids are built from two coat proteins, a 24 kDa small (S) coat protein and a 42 kDa large (L) coat protein. The S and L form an asymmetric unit and 60 copies each form a capsid with pT = 3 symmetry. TRSV has also pT3 symmetry but is assembled from 60 identical copies of a 57 kDa protein (Figure 3A).

Native and denaturing gel electrophoresis were performed; in native agarose gels, all viral nanoparticles migrate toward the anode as a function of their overall negative charge (see Table in Figure 3). CPMV is the most negatively charged and has higher electrophoretic mobility compared to less negatively charged CPSMV and TRSV. TRSV has negligible mobility in the agarose gel reflecting its low negative charge density (Figure 3B). For CPMV and CPSMV, distinct protein bands and RNA bands were observed—the co-localization indicates stable RNA packaging inside the viral capsids. TRSV showed a protein band near the loading well and a higher mobility RNA smear, which may indicate RNA contamination or escape of the RNA during the electrophoretic separation—the latter is plausible because the capsid itself has negligible electrophoretic mobility and RNA contaminants were not apparent by SEC analysis (see Figure 3D). The coat proteins were then separated and analyzed by denaturing gel electrophoresis and western blotting using polyclonal sera raised in mice. For CPMV and CPSMV, both the S and L protein were detected after CoomassieBlue staining as well as in immunoblots after probing with polyclonal mouse antisera. For TRSV, the coat protein at 57 kDa as well as smaller degradation products could be observed after CoomassieBlue staining as well as in immunoblots (Figure 3C). Because antisera recognize the lower molecular weight proteins, we attribute these to degradation products rather than contaminants; however, more research is required to understand the stability of the various formulations.

Lastly, particle integrity was determined using SEC and TEM (Figure 3D,E). Each particle showed the expected elution profile with elution at ~ 11 mL from the Superose 6 column; protein (detected at 280 nm) and RNA (detected at 260 nm) co-eluate, therefore indicating that intact and pure virus preparations were obtained. Each particle has a characteristic 260 nm/280 nm ratio with 1.8–1.9 for CPMV and 1.6–1.7 for CPSMV and TRSV. The measured 260:280 ratio for CPMV and CPSMV is in agreement with description of plant viruses (DPV, dpvweb.net) entries. The measured 260:280 ratio for TRSV is higher than expected—as per DPV, the ratio was reported as A260/A280: 0.72 (T), 1.38 (M), 1.57 (B)—averaging as ~1.5 for the B and M component; this may be in line with protein degradation as noted by SDS-PAGE. SEC indicated a minor fraction of CPMV and CPSMV to be aggregated as evident by the ~9 mL elution peak; TRSV appeared to have a slightly higher degree of aggregation. Nevertheless, TEM imaging indicates that pure and mono-dispersed plant virus nanoparticles were produced with 30 nm diameter and particles appeared uniform in TEM.

Cross-Reactivity of Murine Sera against Plant Secoviridae and Their Interaction with Vimentin.

To assess potential cross-reactivity between antibodies against each plant virus, murine sera were tested in an immunoblot. Only the respective virus with which the mice were immunized was detected, no cross-reactivity was detected between the three sera (Figure 4A)—attesting to the differences in epitopes for each virus particle. For CPMV as well as CPSMV, both coat proteins at 42 and 24 kDa, respectively, were visible. For TRSV, the single coat protein around 57 kDa could be detected. All three sera also detected aggregated forms of coat proteins visible as a smear above the largest coat protein. As no cross-reactivity could be detected, we used the obtained murine sera for characterization of particles and further experiments.

Even though CPMV is a plant virus, it shares structural similarities with animal picornaviruses and was shown to bind to the mammalian protein vimentin.[31] Whether vimentin-binding plays a role in the potent efficacy of the CPMV-ISV is not yet clear, however, given this unique interaction, we sought to test whether CPSMV and TRSV share this feature. Indeed, VOBPA western and dot blots confirm that all three plant viruses bind to vimentin (Figure 4B). In all three plant virus samples binding to vimentin could be observed in a similar manner, at 57 kDa for monomeric vimentin as well as at higher molecular aggregates.

Given that all three of these plant viruses interact with vimentin, we saw this as an opportunity to probe whether vimentin interactions are indeed crucial for the demonstrated potency of CPMV. One strategy was to use vimentin blocking antibodies to inhibit binding of virus to vimentin; however, effective blocking was not achieved, and so, the data were inconclusive. In brief, in in vitro competition binding assays, CPMV–vimentin binding was only partially inhibited by use of blocking antibodies (mAb v9 or 84–1, the latter is specific to bind surface vimentin; Figure S5). Data and methods are shown in the Supporting Information. We also probed whether any differences in efficacy were observed when CPMV was co-administered with mAb v9 or 84–1; however, CPMV maintained its potent efficacy in the B16F10 dermal melanoma model and there were no differences between the CPMV solo vs CPMV + anti-vimentin antibody groups (Figure S6). Because vimentin blocking is only partial, this data do not eliminate or support a contribution of the CPMV–vimentin interactions to the immune response. It is possible that binding to vimentin may enhance tumor residence time and therefore prolonging the immuno–modulatory activity in the TME—this is based on observations from an earlier work where different viruses were tested as in situ vaccination candidates: we observed no immunomodulatory effects of physalis mosaic virus-like particles—which do not interact with vimentin, while some immunomodulatory effects were observed for sesbania mosaic virus—which does interact with vimentin.[28] Studies detailing the intratumoral longevity and fate of CPMV vs other plant viruses are needed to further elucidate this point.

Lastly, we attempted to generate vimentin-binding VLPs based on a bacteriophage that naturally does not bind to vimentin. In brief, vimentin-binding peptides were chemically conjugated to the VLPs; while we confirmed that the peptides recognize and bind to vimentin, negligible binding to vimentin was achieved for the engineered VLP formulations

(see Figure S7). More research and alternate approaches are needed to probe the relevance of the CPMV–vimentin interactions.

Efficacy and Mechanism of Action of ISV Using Plant Picornavirales in Murine Melanoma Model.

ISV has been recognized as a cancer immunotherapy strategy: here the immunostimulatory agent (in our case the plant virus) is administered directly into an identified tumor to reverse local immunosuppression, recruit and active innate immune cells to initiate tumor cell killing, thus leading to processing of TAAs and neoantigens and priming of systemic anti-tumor immunity.[11] We established CPMV as a potent ISV, that is the intratumoral administration of CPMV primes systemic anti-tumor immunity through innate immune activation.[17,22] To test comparative in situ vaccination efficacy of this trio of plant picornaviruses against the well-established B16F10 melanoma model in mice we implanted melanoma cells orthotopically into the skin of syngeneic C57Bl6/J mice. In situ vaccination was done by injecting the plant viruses directly into the tumor. CPMV, TRSV and CPSMV all showed significant anti-tumor efficacy in B16F10 model. However, CPMV had stronger efficacy compared to its counterparts, TRSV and CPSMV (Figure 5). At day 16 post-treatment, tumors did not progress in the CPMV-treated group; at day 30 post-treatment, all mice were alive in the CPMV group (Figure 5A,B). The observed potent efficacy of CPMV is in agreement with prior reports.[17,22,55] It is also of note that the CPMV group showed a high degree of consistency with negligible variability observed when analyzing tumor growth curves from individual animals (Figure 5C). This is in stark contrast to tumor growth curves from animals treated with CPSMV and TRSV where a higher degree of variability in response is observed, also tumors progressed albeit more slowly than the PBS treated control group (Figure 5C). At completion of the study (30 days after first treatment), 20% of CPSMV and 40% of TRSV-treated animals remained alive (vs 100% of CPMV treated animals being alive) (Figure 5A,B).

To investigate why CPMV is more efficacious than CPSMV and TRSV, we hypothesized that changes in cell phenotypes in tumor DLNs could be important. We first extracted and cultured cells from DLNs of B16F10-tumor bearing mice at different time points (24 h and 96 h after the first and second intratumoral treatments). After 24 h incubation in RPMI media with no other in vitro stimulation using CPMV, CPSMV or TRSV, the conditioned medium was tested with ELISAs to determine the concentration of IL-6, IFNβ and IFNγ. Surprisingly, DLN cells collected 24 h after the first treatment had only modest cytokine induction by any of the viruses, and CPMV specifically did not induce higher secretion of IL-6, IFNγ or IFNβ by cells from DLNs (Figure 6A,C,E, left panel). However, the medium conditioned by DLNs extracted from mice 96 h after first injection showed a significant increase of IL-6, IFNγ, and IFNβ by CPMV as compared to CPSMV or TRSV (Figure 6A,C,E, right panel). Similarly, but with even larger differences, a similar pattern was observed in DLNs extracted from mouse 24 h and 96 h after the second dosing (Figure 6B,D,F). Again at 24 h, there were modest cytokine inductions, but at 96 h after the second treatment, CPMV induced levels of cytokines that were many-fold higher than any other virus. Quite notably, after DLN cells from CPMV treated animals cultured 96 h after the second treatment also had at least 3-fold higher cytokine levels in comparison to 96 h

after the first treatment. This notably increased cytokine generation by DLN cells clearly demonstrates mechanistically relevant changes in the DLN that are mediated exclusively by CPMV. The slow developing and prolonged impact of these DLN cell changes provides cellular mechanism that helps explain why CPMV is more efficacious than the other two viruses.

This agrees with earlier work in which we compared CPMV with TMV;[16] data indicated that while TMV elicits a pro-inflammatory response within the tumor upon injection, it does not establish a long-lasting response and the response is not higher after a second dose. In stark contrast, the onset of the CPMV-induced cytokine/chemokine profile was notably delayed and distinct, likely due to initial recruitment and/or reprogramming of immune cells, which in turn mount more potent antitumor immunity.[16]

Our next goal was to explain the observation from the perspective of cellular recognition of the reagents. As illustrated by our previous study, CPMV is a multi-TLR agonist for TLRs 2, 4, and 7 and part of its superior anti-tumor efficacy is contributed by the additional type I interferons[22] induced by TLR 7 stimulations. Thus, we proposed the hypothesis that CPSMV and TRSV, just like CPMV, may also be TLR agonists; the superior efficacy of CPMV compared to the other two viruses may also be attributed to difference in TLR stimulations. To confirm this hypothesis, we utilized the splenocyte assays previously established.[22] We first confirmed that the recognitions of CPMV, CPSMV and TRSV all required MyD88 (Figure 7A,B), a central adaptor of TLR signaling pathway.[56] As shown in Figure 7A,B, the induction of IL-6 and IFNβ by CPMV, CPSMV and TRSV was completely abolished in MyD88 KO mouse splenocyte assay. Furthermore, CPMV induced significantly more IFNβ than CPSMV and TRSV (Figure 7B). Since type I interferons are critical for anti-tumor efficacy,[57] this may provide an explanation for why CPMV showed superior anti-tumor efficacy than TRSV and CPSMV.

Next, we investigated the involvement of TLRs 2, 4, and 7 for CPSMV and TRSV recognition by exposing mouse splenocytes to the viruses in vitro. All cytokine induction required the TLR signaling molecule MyD88; so as previously shown for CPMV, MyD88 is necessary for recognition of CPSMV and TRSV. The trend of IL-6 induction by CPMV, CPSMV and TRSV stayed the same in TLR2, TLR4, and TLR7 KO mice, although had reduced IL-6 compared to wild type mice (Figure 7A,C,E). However, unlike the IL-6 induction, the superior induction of IFNβ by CPMV vanished in TLR7 KO in which all three viruses then induced IFNβ at the same extent (Figure 7B,D,F). This aligns with our previous finding that CPMV is a TLR7 agonist which is critical for induction of type I IFN and this may be a key differentiator for the superior anti-tumor efficacy of CPMV-ISV.[22]

CONCLUSIONS

In this work, we compared the efficacy of plant viruses from the Secoviridea for use as ISV. The three viruses under investigation, CPMV, CPSMV, and TRSV share similarities in their structural features, in that they form three isometric capsids that package one or the other molecule of the bipartite RNA genome or no RNA. The capsids measure ~30 nm in size have a net negative charge and pT = 3 symmetry. CPSMV and CPMV have homology in

their genome and coat protein sequences, while TRSV lacks homology to CPMV. When applied as ISV using a dermal melanoma mouse model, only CPMV demonstrated potent efficacy with all CPMV-treated animals responding to the treatment. In contrast, CPSMV and TRSV showed some efficacy—with a greater degree of variability between individual animals and only 20 or 40% remaining in the study at the time point of completion—100% of the CPMV-treated animals were alive at the study conclusion. Immunological mechanism studies indicate that all three plant viruses are indeed immunogenic and signal through PRRs requiring MyD88—the key differentiator is that CPSMV and TRSV predominantly signal through TLRs 2 and 4, while CPMV signals also through TLR7 leading to IFNβ signaling. We therefore attribute IFNβ released upon TLR7 activation as a key contributor for the observed potency of CPMV-ISV. Another clear difference in response to CPMV was the increase of cytokine expression in vivo over 4 days. While cytokines from CPSMV and TRSV had clearly fallen back to baseline by 4 days after treatment, those from CPMV had increased. Similarly, 4 days after the second treatment with CPMV, the cytokine response was multiple-fold higher than after the first treatment at that time point, while again, response to CPSMV and TRSV were equal to PBS. This delayed but higher immune response and apparent increase with multiple treatments is a significant mechanistic insight into why CPMV has exceptional efficacy.

We also probed the CPMV–vimentin interaction; however, the mechanistic involvement of vimentin binding remains unclear. One may argue that the CPMV–vimentin interaction is critical for the observed potency—however, CPSMV and TRSV also interact with vimentin yet do not reach potency as observed for CPMV. Probing the role of vimentin for the CPMV-ISV however has been technically challenging.

The high potency of the CPMV-ISV is intriguing and requires further investigation. It is plausible that either the CPMV genome contains key signatures for TLR7 activation that other plant viruses lack; or that CPMV trafficking and unpacking of the RNA differs and is unique in a way allowing more efficient TLR7 engagement. Further, the apparent stronger response to CPMV after previous exposure suggests lymphocyte involvement, either by generation of T cell or B cell responses or both—and this may be explained by unique T helper epitopes within the coat protein. These multiple hypotheses are currently being investigated in our laboratories and results will be reported elsewhere. We envision CPSMV and TRSV to be suitable tools to probe the mechanism and uniqueness of the CPMV-ISV.

Supplementary Material

Refer to Web version on PubMed Central for supplementary material.

ACKNOWLEDGMENTS

This work was funded in part by the following grants from the National Institute of Health (NIH) (U01-CA218292 to N.F.S. and S.F. and R01-CA224605 to N.F.S. and R01 CA253615 to N.F.S. and S.F.), CDMRP (W81XWH2010742 to N.F.S.). Dr. Zhongchao Zhao (UC San Diego) is thanked for helpful discussions regarding structural analysis and help with building the model of CPSMV. We thank Matthew D. Shin (UC San Diego) for conjugation of Qβ to the vimentin-binding peptides, Dr. Sourabh Shukla for conjugation of Cy5 to CPMV (UC San Diego), Justin McCaskill for drawings used in Figure 1.

REFERENCES

(1). Hoteit M; Oneissi Z; Reda R; Wakim F; Zaidan A; Farran M; Abi-Khalil E; El-Sibai M Cancer immunotherapy: A comprehensive appraisal of its modes of application (Review). Oncol. Lett 2021, 22, 655. [PubMed: 34386077]

(2). Esfahani K; Roudaia L; Buhlaiga N; Del Rincon SV; Papneja N; Miller WH Jr. A review of cancer immunotherapy: from the past, to the present, to the future. Curr. Oncol 2020, 27, S87–S97. [PubMed: 32368178]

(3). Mohanty R; Chowdhury CR; Arega S; Sen P; Ganguly P; Ganguly N CAR T cell therapy: A new era for cancer treatment (Review). Oncol. Rep 2019, 42, 2183–2195. [PubMed: 31578576]

(4). Hemminki O; Dos Santos JM; Hemminki A Oncolytic viruses for cancer immunotherapy. J. Hematol. Oncol 2020, 13, 84. [PubMed: 32600470]

(5). Bommareddy PK; Shettigar M; Kaufman HL Integrating oncolytic viruses in combination cancer immunotherapy. Nat. Rev. Immunol 2018, 18, 498–513. [PubMed: 29743717]

(6). Larocca C; Schlom J Viral vector-based therapeutic cancer vaccines. Cancer J. 2011, 17, 359–371. [PubMed: 21952287]

(7). Harrop R; John J; Carroll MW Recombinant viral vectors: cancer vaccines. Adv. Drug Delivery Rev 2006, 58, 931–947.

(8). Ribas A; Wolchok JD Cancer immunotherapy using checkpoint blockade. Science 2018, 359, 1350–1355. [PubMed: 29567705]

(9). Urban-Wojciuk Z; Khan MM; Oyler BL; Fåhraeus R; Marek-Trzonkowska N; Nita-Lazar A; Hupp TR; Goodlett DR The Role of TLRs in Anti-cancer Immunity and Tumor Rejection. Front. Immunol 2019, 10, 2388. [PubMed: 31695691]

(10). Pahlavanneshan S; Sayadmanesh A; Ebrahimiyan H; Basiri M Toll-Like Receptor-Based Strategies for Cancer Immunotherapy. J. Immunol. Res 2021, 2021, 9912188. [PubMed: 34124272]

(11). Sheen MR; Fiering S In situ vaccination: Harvesting low hanging fruit on the cancer immunotherapy tree. Wiley Interdiscip. Rev.: Nanomed. Nanobiotechnol 2019, 11, No. e1524. [PubMed: 29667346]

(12). Gromeier M; Nair SK Recombinant Poliovirus for Cancer Immunotherapy. Annu. Rev. Med 2018, 69, 289–299. [PubMed: 29414253]

(13). Pol J; Buqué A; Aranda F; Bloy N; Cremer I; Eggermont A; Erbs P; Fucikova J; Galon J; Limacher J-M; Preville X; Sautès-Fridman C; Spisek R; Zitvogel L; Kroemer G; Galluzzi L Trial Watch-Oncolytic viruses and cancer therapy. Oncoimmunology 2016, 5, No. e1117740. [PubMed: 27057469]

(14). Bubna A Imiquimod - Its role in the treatment of cutaneous malignancies. Indian J. Pharmacol 2015, 47, 354–359. [PubMed: 26288465]

(15). Mohsen MO; Speiser DE; Knuth A; Bachmann MF Virus-Like Particles for Vaccination against Cancer; Wiley Interdiscip Rev Nanomed Nanobiotechnol, 2019; p e1579. [PubMed: 31456339]

(16). Murray AA; Wang C; Fiering S; Steinmetz NF In Situ Vaccination with Cowpea vs Tobacco Mosaic Virus against Melanoma. Mol. Pharm 2018, 15, 3700–3716. [PubMed: 29798673]

(17). Lizotte PH; Wen AM; Sheen MR; Fields J; Rojanasopondist P; Steinmetz NF; Fiering S In situ vaccination with cowpea mosaic virus nanoparticles suppresses metastatic cancer. Nat. Nanotechnol 2016, 11, 295–303. [PubMed: 26689376]

(18). Kerstetter-Fogle A; Shukla S; Wang C; Beiss V; Harris PLR; Sloan AE; Steinmetz NF Plant Virus-Like Particle In Situ Vaccine for Intracranial Glioma Immunotherapy. Cancers 2019, 11, 515.

(19). Hoopes PJ; Mazur CM; Osterberg B; Song A; Gladstone DJ; Steinmetz NF; Veliz FA; Bursey AA; Wagner RJ; Fiering SN Effect of intra-tumoral magnetic nanoparticle hyperthermia and viral nanoparticle immunogenicity on primary and metastatic cancer. Proc. SPIE-Int. Soc. Opt. Eng 2017, 10066, 100660G.

(20). Hoopes PJ; Moodie KL; Petryk AA; Petryk JD; Sechrist S; Gladstone DJ; Steinmetz NF; Veliz FA; Bursey AA; Wagner RJ; Rajan A; Dugat D; Crary-Burney M; Fiering SN Hypo-fractionated Radiation, Magnetic Nanoparticle Hyperthermia and a Viral Immunotherapy Treatment of

Spontaneous Canine Cancer. Proc. SPIE-Int. Soc. Opt. Eng 2017, 10066, 1006605. [PubMed: 29203951]

(21). Hoopes PJ; Wagner RJ; Duval K; Kang K; Gladstone DJ; Moodie KL; Crary-Burney M; Ariaspulido H; Veliz FA; Steinmetz NF; Fiering SN Treatment of Canine Oral Melanoma with Nanotechnology-Based Immunotherapy and Radiation. Mol. Pharm 2018, 15, 3717–3722. [PubMed: 29613803]

(22). Mao C; Beiss V; Fields J; Steinmetz NF; Fiering S Cowpea mosaic virus stimulates antitumor immunity through recognition by multiple MYD88-dependent toll-like receptors. Biomaterials 2021, 275, 120914. [PubMed: 34126409]

(23). Wang C; Beiss V; Steinmetz NF Cowpea Mosaic Virus Nanoparticles and Empty Virus-Like Particles Show Distinct but Overlapping Immunostimulatory Properties. J. Virol 2019, 93, No. e00129–19. [PubMed: 31375592]

(24). Wang C; Fiering SN; Steinmetz NF Cowpea Mosaic Virus Promotes Anti-Tumor Activity and Immune Memory in a Mouse Ovarian Tumor Model. Adv. Ther 2019, 2, 1900003.

(25). Patel R; Czapar AE; Fiering S; Oleinick NL; Steinmetz NF Radiation Therapy Combined with Cowpea Mosaic Virus Nanoparticle in Situ Vaccination Initiates Immune-Mediated Tumor Regression. ACS Omega 2018, 3, 3702–3707. [PubMed: 29732445]

(26). Cai H; Wang C; Shukla S; Steinmetz NF Cowpea Mosaic Virus Immunotherapy Combined with Cyclophosphamide Reduces Breast Cancer Tumor Burden and Inhibits Lung Metastasis. Adv. Sci 2019, 6, 1802281.

(27). Wang C; Steinmetz NF A Combination of Cowpea mosaic virus and Immune Checkpoint Therapy Synergistically Improves Therapeutic Efficacy in Three Tumor Models. Adv. Funct. Mater 2020, 30, 2002299. [PubMed: 34366758]

(28). Shukla S; Wang C; Beiss V; Cai H; Washington T 2nd; Murray AA; Gong X; Zhao Z; Masarapu H; Zlotnick A; Fiering S; Steinmetz NF The unique potency of Cowpea mosaic virus (CPMV) in situ cancer vaccine. Biomater. Sci 2020, 8, 5489–5503. [PubMed: 32914796]

(29). Stump CT; Ho G; Mao C; Veliz FA; Beiss V; Fields J; Steinmetz NF; Fiering S Remission-Stage Ovarian Cancer Cell Vaccine with Cowpea Mosaic Virus Adjuvant Prevents Tumor Growth. Cancers 2021, 13, 627. [PubMed: 33562450]

(30). Lee KL; Murray AA; Le DHT; Sheen MR; Shukla S; Commandeur U; Fiering S; Steinmetz NF Combination of Plant Virus Nanoparticle-Based in Situ Vaccination with Chemotherapy Potentiates Antitumor Response. Nano Lett. 2017, 17, 4019–4028. [PubMed: 28650644]

(31). Koudelka KJ; Destito G; Plummer EM; Trauger SA; Siuzdak G; Manchester M Endothelial targeting of cowpea mosaic virus (CPMV) via surface vimentin. PLoS Pathog. 2009, 5, No. e1000417. [PubMed: 19412526]

(32). Sali A; Blundell TL Comparative protein modelling by satisfaction of spatial restraints. J. Mol. Biol 1993, 234, 779–815. [PubMed: 8254673]

(33). Pettersen EF; Goddard TD; Huang CC; Couch GS; Greenblatt DM; Meng EC; Ferrin TE UCSF Chimera?A visualization system for exploratory research and analysis. J. Comput. Chem 2004, 25, 1605–1612. [PubMed: 15264254]

(34). Wellink J Comovirus isolation and RNA extraction. Methods Mol. Biol 1998, 81, 205–209. [PubMed: 9760508]

(35). Chariou PL; Beiss V; Ma Y; Steinmetz NF In situ vaccine application of inactivated CPMV nanoparticles for cancer immunotherapy. Mater. Adv 2021, 2, 1644–1656. [PubMed: 34368764]

(36). Lomonossoff GP; Shanks M The nucleotide sequence of cowpea mosaic virus B RNA. EMBO J. 1983, 2, 2253–2258. [PubMed: 16453487]

(37). van Wezenbeek P; Verver J; Harmsen J; Vos P; van Kammen A Primary structure and gene organization of the middle-component RNA of cowpea mosaic virus. EMBO J. 1983, 2, 941–946. [PubMed: 6641721]

(38). Bruening G; Agrawal HO Infectivity of a mixture of cowpea mosaic virus ribonucleoprotein components. Virology 1967, 32, 306–320. [PubMed: 4960987]

(39). Stanley J; Rottier P; Davies JW; Zabel P; van Kammen A A protein linked to the 5′ termini of both RNA components of the cowpea mosaic virus genome. Nucleic Acids Res. 1978, 5, 4505–4522. [PubMed: 745988]

(40). Daubert SD; Bruening G; Najarian RC Protein bound to the genome RNAs of cowpea mosaic virus. Eur. J. Biochem 1978, 92, 45–51. [PubMed: 215411]

(41). El Manna MM; Bruening G Polyadenylate sequences in the ribonucleic acids of cowpea mosaic virus. Virology 1973, 56, 198–206. [PubMed: 4745624]

(42). Davies JW; Aalbers AMJ; Stuik EJ; Van Kammen A Translation of cowpea mosaic virus RNA in a cell-free extract from wheat germ. FEBS Lett. 1977, 77, 265–269. [PubMed: 862928]

(43). Pelham HRB Synthesis and proteolytic processing of cowpea mosaic virus proteins in reticulocyte lysates. Virology 1979, 96, 463–477. [PubMed: 462814]

(44). Goldbach RW; Schilthuis JG; Rezelman G Comparison of in vivo and in vitro translation of cowpea mosaic virus RNAs. Biochem. Biophys. Res. Commun 1981, 99, 89–94. [PubMed: 7236272]

(45). Goldbach R; Rezelman G; van Kammen A Independent replication and expression of B-component RNA of cowpea mosaic virus. Nature 1980, 286, 297–300.

(46). Gopo JM; Frist RH Location of the gene specifying the smaller protein of the cowpea mosaic virus capsid. Virology 1977, 79, 259–266. [PubMed: 867824]

(47). Thongmeearkom P; Goodman RM Complementation and pseudorecombination between ribonucleic acids from two natural isolates of cowpea mosaic virus (severe subgroup). Virology 1978, 85, 75–83. [PubMed: 77077]

(48). Bancroft JB Purification and properties of bean pod mottle virus and associated centrifugal and electrophoretic components. Virology 1962, 16, 419–427. [PubMed: 13864586]

(49). Wu G-J; Bruening G Two proteins from cowpea mosaic virus. Virology 1971, 46, 596–612. [PubMed: 5137799]

(50). Lomonossoff GP; Johnson JE The synthesis and structure of comovirus capsids. Prog. Biophys. Mol. Biol 1991, 55, 107–137. [PubMed: 1871315]

(51). Chen X; Bruening G Cloned DNA copies of cowpea severe mosaic virus genomic RNAs: infectious transcripts and complete nucleotide sequence of RNA 1. Virology 1992, 191, 607–618. [PubMed: 1448917]

(52). Chen X; Bruening G Nucleotide sequence and genetic map of cowpea severe mosaic virus RNA 2 and comparisons with RNA 2 of other comoviruses. Virology 1992, 187, 682–692. [PubMed: 1546463]

(53). Zalloua PA; Buzayan JM; Bruening G Chemical cleavage of 5’-linked protein from tobacco ringspot virus genomic RNAs and characterization of the protein-RNA linkage. Virology 1996, 219, 1–8. [PubMed: 8623518]

(54). Komatsu K; Hashimoto M; Ozeki J; Yamaji Y; Maejima K; Senshu H; Himeno M; Okano Y; Kagiwada S; Namba S Viral-induced systemic necrosis in plants involves both programmed cell death and the inhibition of viral multiplication, which are regulated by independent pathways. Mol. Plant-Microbe Interact 2010, 23, 283–293. [PubMed: 20121450]

(55). Wang C; Steinmetz NF A Combination of Cowpea Mosaic Virus and Immune Checkpoint Therapy Synergistically Improves Therapeutic Efficacy in Three Tumor Models. Adv. Funct. Mater 2020, 30, 2002299. [PubMed: 34366758]

(56). Akira S; Takeda K Functions of toll-like receptors: lessons from KO mice. Comptes Rendus Biol. 2004, 327, 581–589.

(57). Zitvogel L; Galluzzi L; Kepp O; Smyth MJ; Kroemer G Type I interferons in anticancer immunity. Nat. Rev. Immunol 2015, 15, 405–414. [PubMed: 26027717]

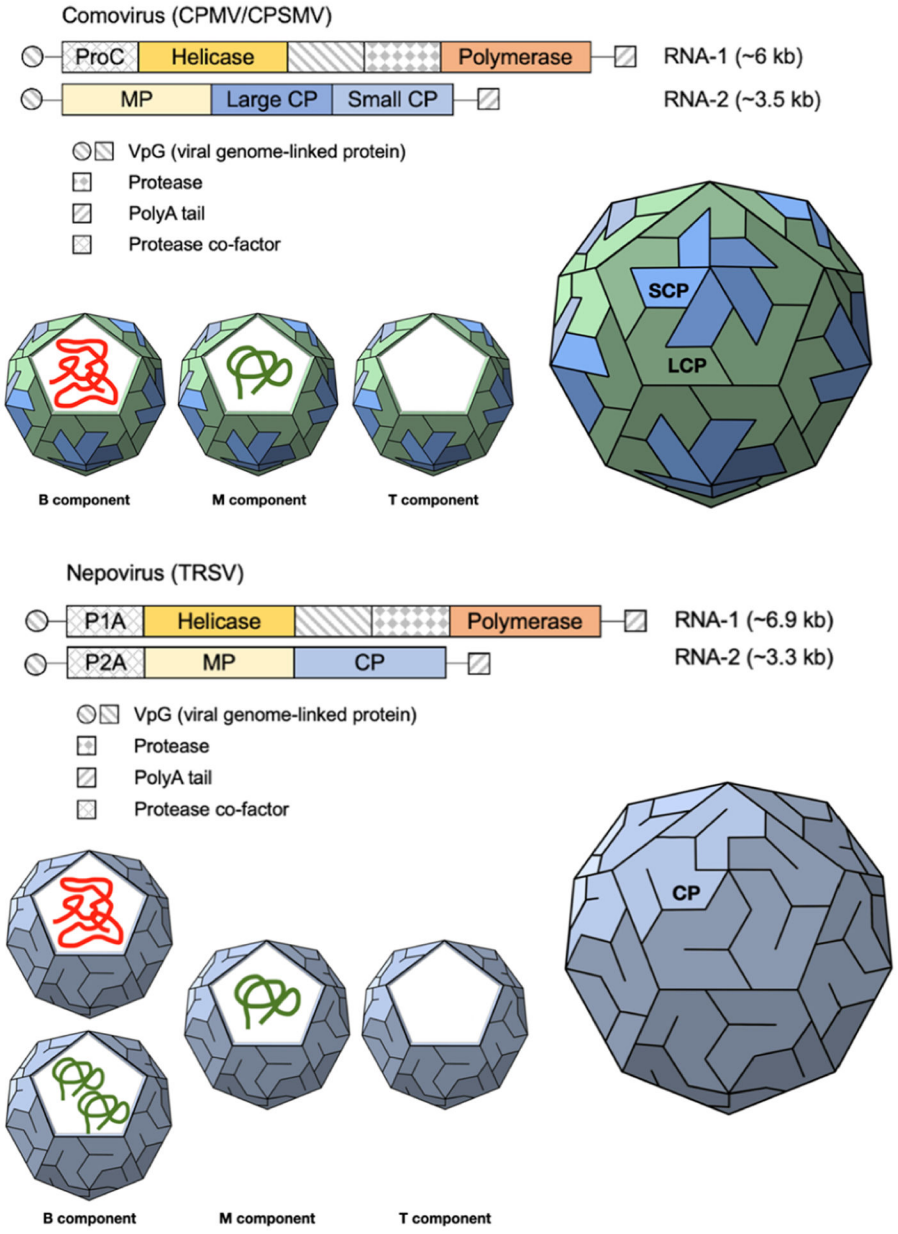

Figure 1.

Genome organization and RNA packaging of comoviruses CPMV and CPSMV and nepovirus TRSV. ProC/P1A/P2A: Protease co-factors, MP: movement protein, CP: coat protein. Genome organization according to https://viralzone.expasy.org/300 and https://viralzone.expasy.org/298?outline=all_by_species. Capsid structures drawn by Justin McCaskill (UC San Diego).

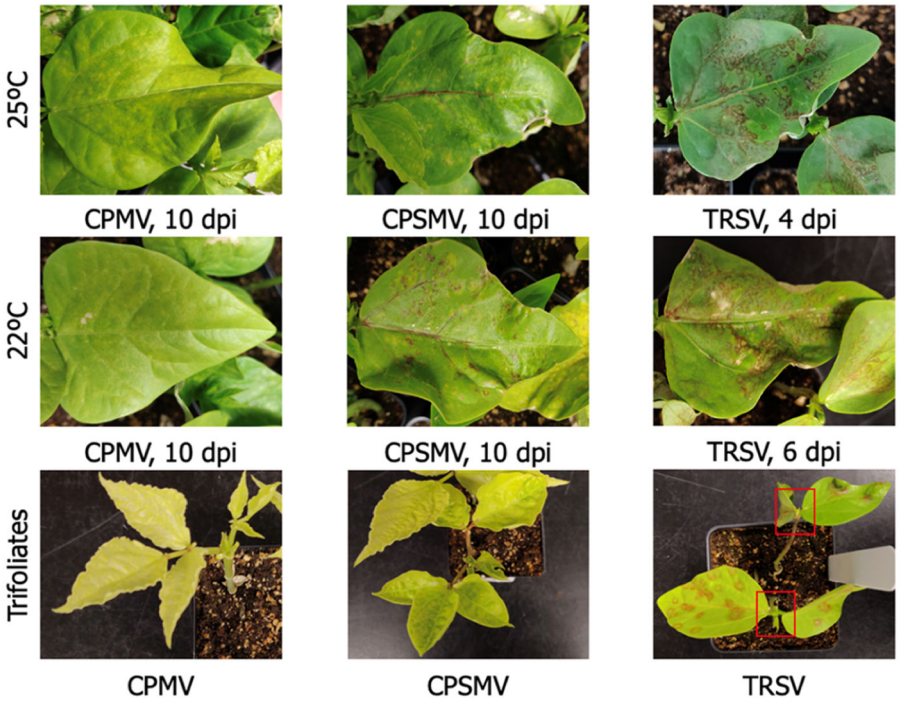

	CPMV	CPSMV	TRSV
Purification	Grind leaves with 2-3 vol 0.1 M KP, filter, centrifuge for 20 mins at 18,500 g Add 0.7 vol 1:1 chloroform:butanol and mix on ice for 20 mins followed by centrifugation for 10 mins at 6,600 g, collect upper aqueous phase Add 0.2 M NaCl, 8-10% PEG, stir on ice for 30 mins, let sit at 4°C for at least 2 h or overnight Centrifuge for 15 mins at 30,000 g, resuspend pellet in 10 mL 0.01 M KP Centrifuge for 15 mins at 13,500 g, collect supernatant Purify supernatant over 10-40% sucrose gradient for 2.5-3 h at 120,000 g, collect virus fraction (light scattering band of the B and M component) Centrifuge collected bands for 2.5-3 h at 200,000 g, resuspend pellet in 1-2 mL 0.1 M KP Dialyze sample against 0.1 M KP, characterize, store at 4°C until further use		
Yields	0.5-0.9 mg/g	0.2-0.5 mg/g	0.05-0.2 mg/g
Symptoms	Yellow to light green mosaic spots, trifoliates with mosaic pattern.	Yellow to red-brown to yellow mosaic spots, leaf veins discolored to red-brown. Trifoliates blistered and distorted. Slight necrosis on stem.	Red-brown necrotic spots, leaf veins discolored, severe necrosis and wilting. Trifoliates may not develop.

Figure 2.

Symptoms of CPMV, CPSMV, and TRSV in *V. unguiculata*. Primary leaves are shown 10 days post-inoculation (dpi) for CPMV and CPSMV; and 4–6 dpi for TRSV; trifoliates (secondary leaves) are shown at day 16 for CPMV- and CPSMV-infected plants and day 10 for TRSV-infected plants. Note: to show any secondary leaves in TRSV-infected plants (see red square), a plant with mild symptoms was chosen. Plants were maintained at 22 or 25 °C. The purification protocol (primary leaves were harvested and virus was extracted) was identical for all three plant viruses with yields varying from 0.05–0.2 mg TRSV/gram of leaf tissue up to 0.5–0.9 mg of CPSMV and CPMV per gram infected leaf tissue.

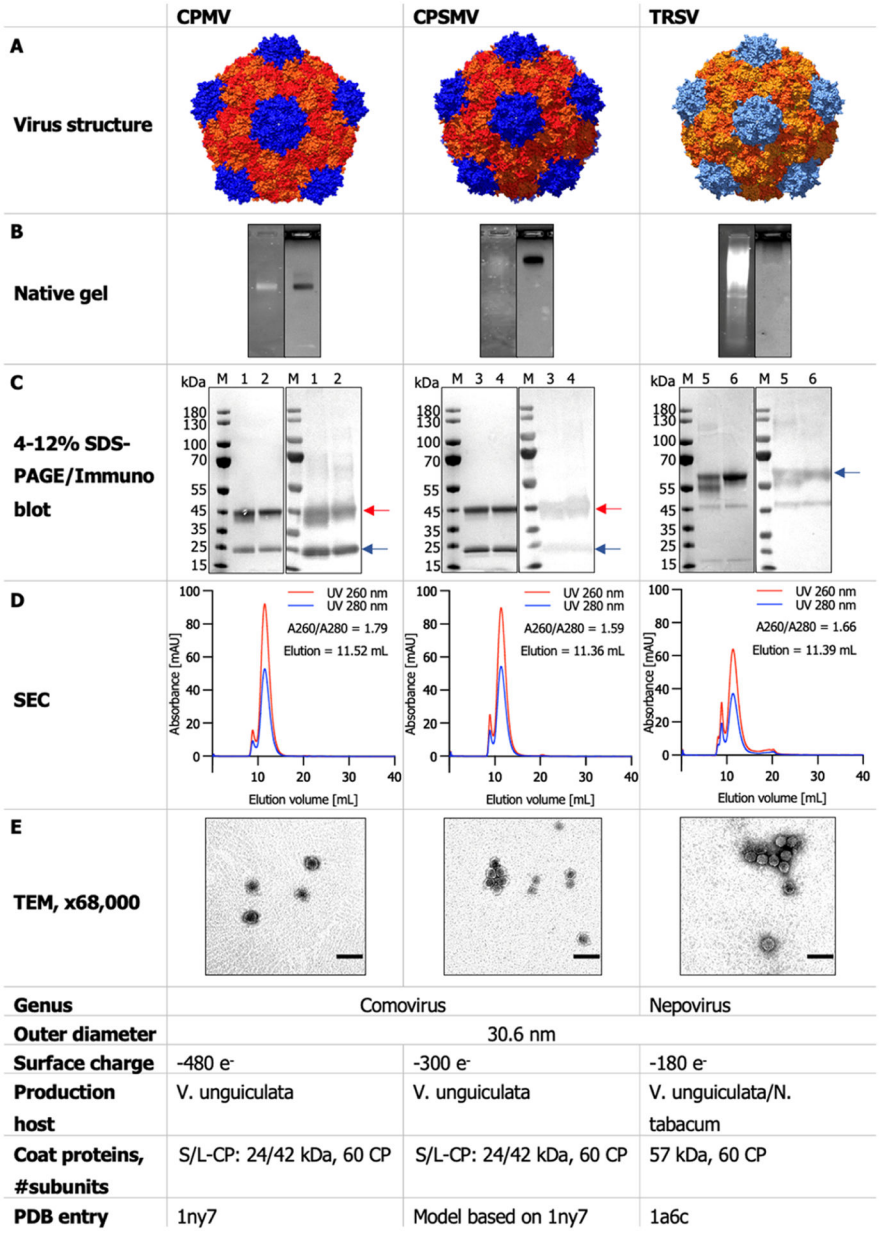

Figure 3.

Characterization of plant picornavirus nanoparticles. Left column: CPMV, middle column: CPSMV, and right column: TRSV. (A) Structure of plant viruses, CPMV, created with Chimera using the Protein Data Bank (PDB) entry 1ny7, CPSMV, modeled based 1ny7 using UniProt entry P31630 and Chimera (see methods), TRSV, created with Chimera using the PDB entry 1a6c. CPMV and CPSMV capsids consist of an L and S protein, the S protein is clustered around the fivefold axis and depicted in blue; the L sits at the two- and threefold axis and folds into two domains colored in two shades of red. TRSV capsids consist of a single CP that folds into three domains, which are colored in blue (fivefold axis) and two shades of orange (two- and threefold axis). (B) Native agarose gel electrophoresis stained with GelRed nucleic acid stain (left) and Coomassie Brilliant Blue (right). (C) Denaturing,

nonreducing (odd lane numbers), and reducing (even lane numbers) 4–12% NuPage gel stained with GelCode Blue Safe protein stain (left) and immunoblot, probed with mouse-αVNP and HRP-labeled goat-α mouse IgG antibodies. (D) SEC analysis showing the characteristic elution profile from a Superose 6 increase 10/300 column. (E) TEM images of negatively stained virus nanoparticles; the scale bar is 50 nm.

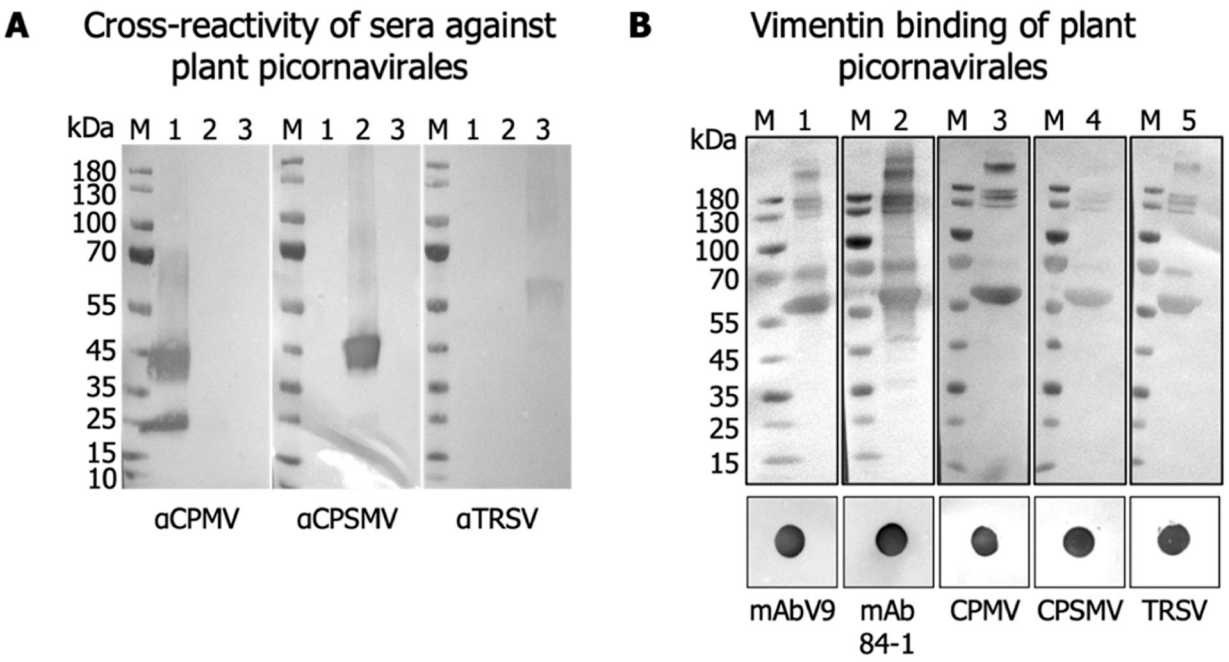

Figure 4.

(A) Cross-reactivity of murine sera against plant picornavirales probed by western blot; 6 μg of 1: CPMV, 2: CPSMV, 3: TRSV, M: Invitrogen PageRuler Prestained Protein Marker. Immunoblots probed with mouse-αCPMV, mouse-αCPSMV, mouse-αTRSV, each 1:1000 diluted. Subsequently, membranes were probed with 1:5000 diluted HRP-labeled goat-α mouse IgG antibody before blots were developed with the DAB substrate (DAB Substrate Kit, Vector Laboratories). (B) VNP-vimentin interactions were probed by VOPBA via western and dot blot. 6 μg of vimentin was probed with 100 μg of VNPs or 2 μg of anti-vimentin antibody after western blotting. 1: 2 μg mAbv9, 2: 2 μg CSV mAb84–1, 3: 100 μg CPMV, 4: 100 μg CPSMV, 5: 100 μg TRSV. VOPBAs were probed with mouse-αCPMV, mouse-αCPSMV, and mouse-αTRSV, each 1:1000 diluted, except when anti-vimentin antibodies were used. Subsequently, membranes were probed with 1:5000 diluted HRP-labeled goat-α mouse IgG antibody before blots were developed with the DAB substrate (DAB Substrate Kit, Vector Laboratories).

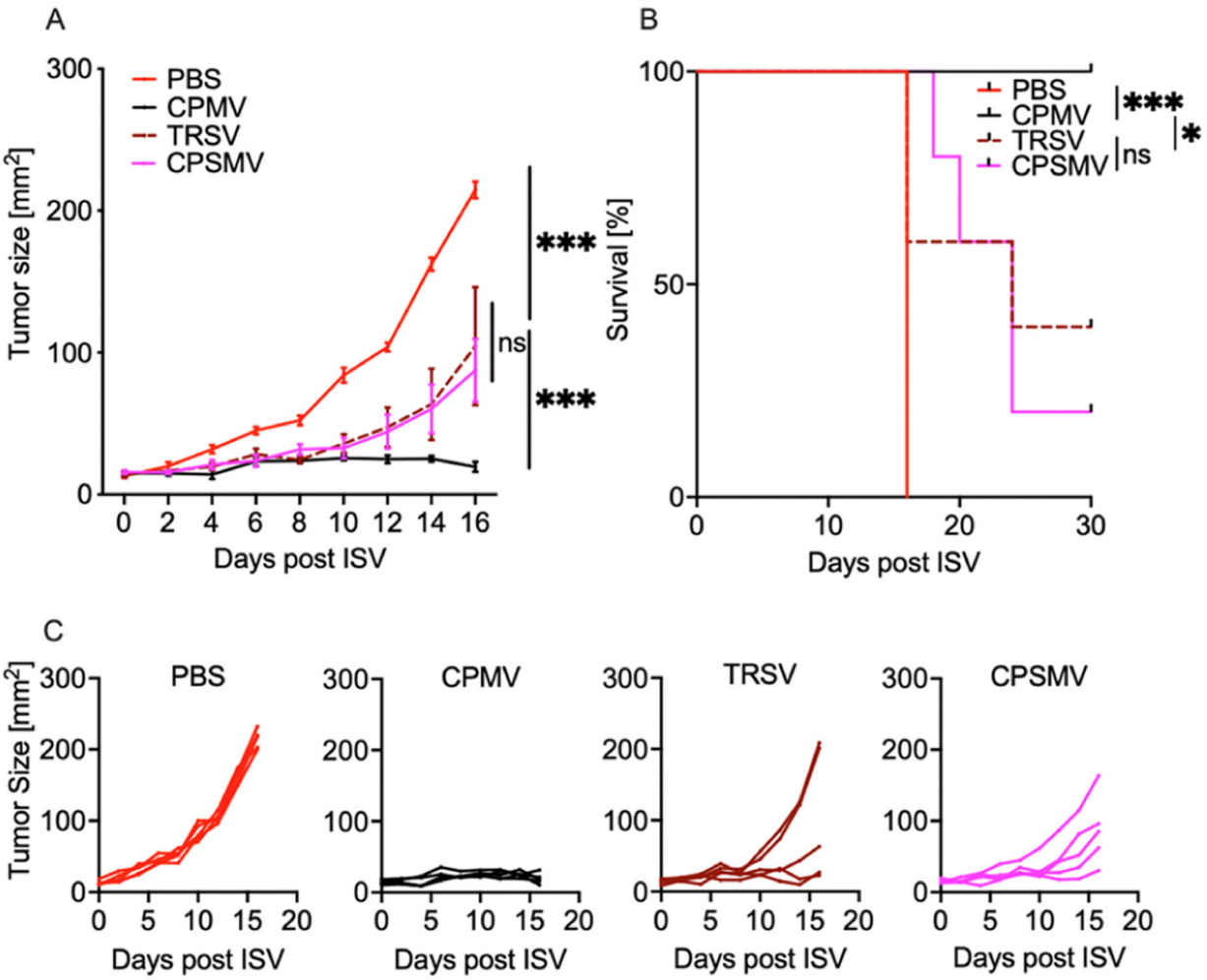

Figure 5.

Anti-tumor efficacy of plant picornaviruses. 1.25×10^5 B16F10 melanoma cells were injected intradermally on day −7 into C57BL6/J mice ($n = 5$). 100 μg CPMV (black), TRSV (brown), or CPSMV (pink) were injected intratumorally on day 0 and day 7. Injection with PBS (red) served as control group. (A) Tumor growth was monitored every other day until 30 days after first treatment and euthanized when the tumor reached a size of 200 mm^2. Tumor progression was monitored by measuring tumor surface area (length × width). (B) Survival curves. (C) Growth curves for each mouse in the study are shown. Growth curves were analyzed using 2-Way ANOVA Survival curves were analyzed using log-rank (Mantel–Cox) test, with $p > 0.05$ as ns, $p < 0.05$ as *, $p < 0.01$ as ** and $p < 0.001$ as ***.

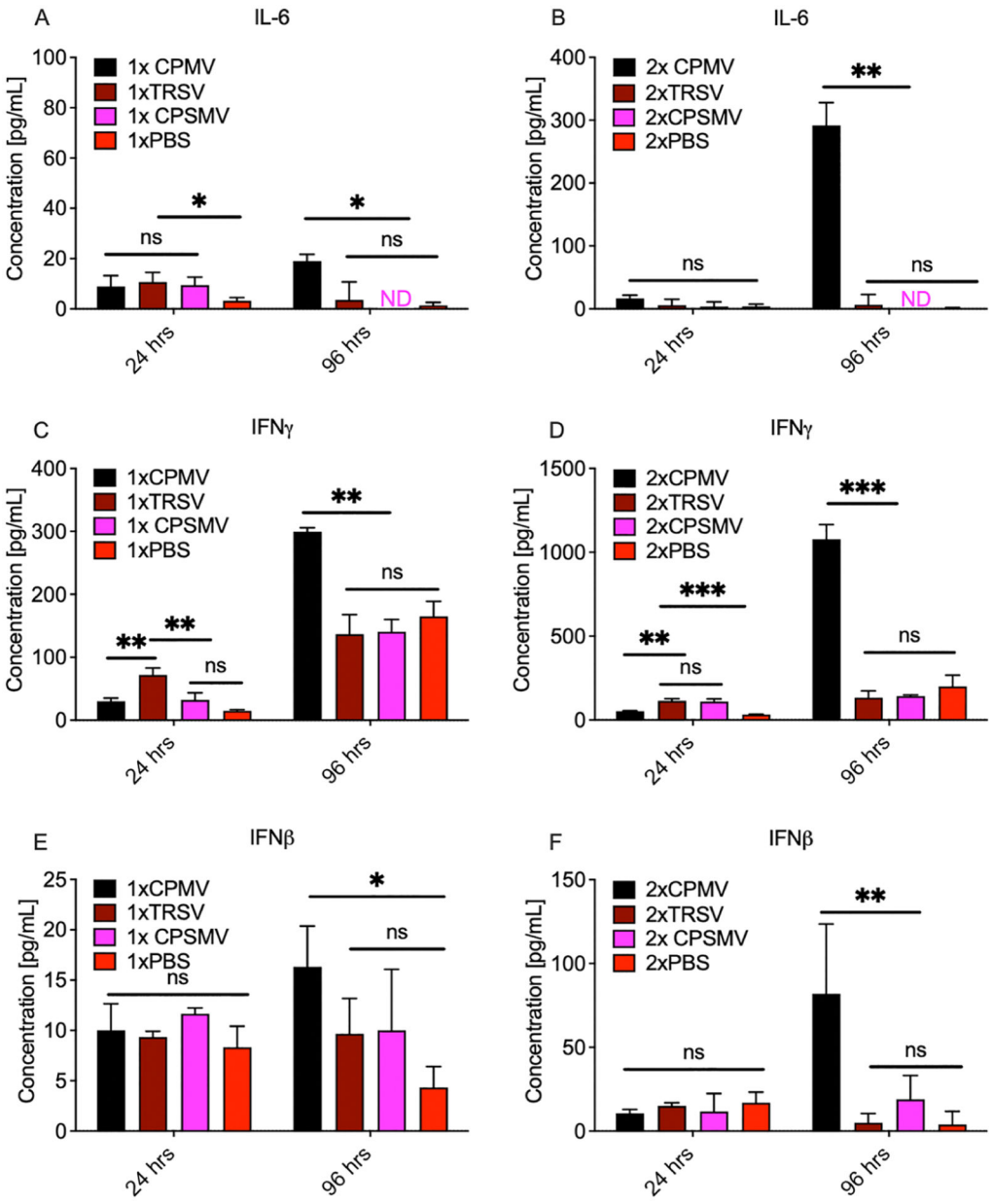

Figure 6.

Induction of pro-inflammatory cytokines after co-culture of CPMV, CPSMV, and TRSV with lymphocytes. DLNs of B16F10 tumor-bearing C57BL/6J (n = 3/treatment) were homogenized and cultured in complete RPMI for 24 h. The conditioned medium was then analyzed with IL-6 (A,B), IFNγ (C,D) and IFNβ (D,E) ELISA at 24 h and 96 h after first (A,C,E) and second treatment (B,D,F). ND not detectable.

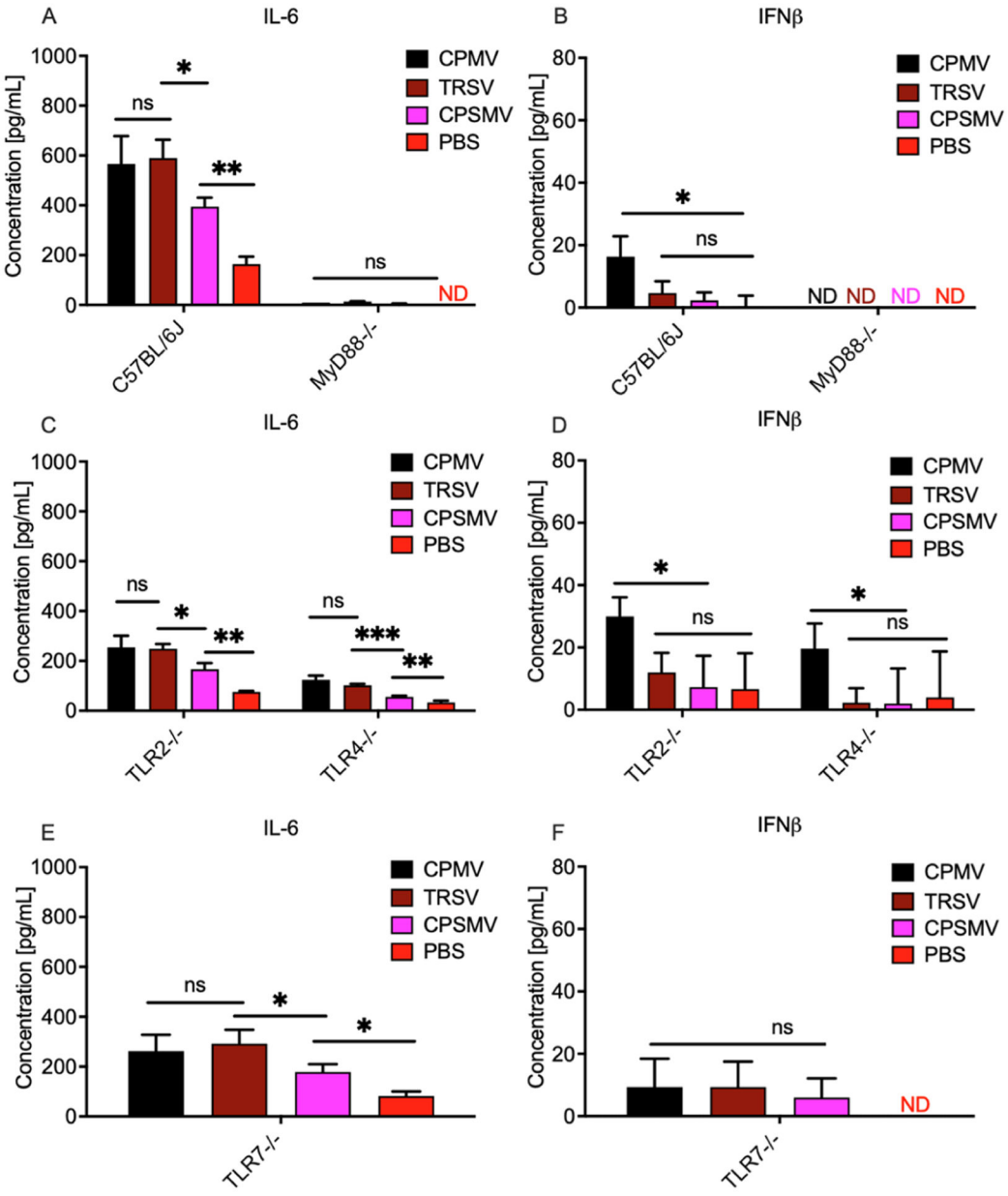

Figure 7.

CPMV, TRSV and CPSMV are recognized through MyD88-dependent TLR. Splenocytes from corresponding transgenic knockout mice ($n = 3$) were cultured for 24 h with CPMV, TRSV, or CPSMV and cytokine levels in supernatants were analyzed with IL-6 (A,C,E) or IFNβ (B,D,F) ELISA. Data for bar graphs calculated using unpaired Student's *t*-test, with $p < 0.05$ as ns, $p < 0.05$ as *, $p < 0.01$ as ** and $p < 0.001$ as ***. ND not detectable.